

ExoMol molecular line lists XXX: a complete high-accuracy line list for water

Oleg L. Polyansky^{1,2}, Aleksandra A. Kyuberis², Nikolai F. Zobov²,
Jonathan Tennyson^{1*}, Sergei N. Yurchenko¹, Lorenzo Lodi¹

¹*Department of Physics and Astronomy, University College London, London WC1E 6BT, UK*

²*Institute of Applied Physics, Russian Academy of Sciences, Ulyanov Street 46, Nizhny Novgorod, Russia 603950.*

Accepted XXXX. Received XXXX; in original form XXXX

ABSTRACT

A new line list for H₂¹⁶O is presented. This line list, which is called POKAZATEL, includes transitions between rotation-vibrational energy levels up to 41 000 cm⁻¹ in energy and is the most complete to date. The potential energy surface (PES) used for producing the line list was obtained by fitting a high-quality *ab initio* PES to experimental energy levels with energies of 41 000 cm⁻¹ and for rotational excitations up to $J = 5$. The final line list comprises all energy levels up to 41 000 cm⁻¹ and rotational angular momentum J up to 72. An accurate *ab initio* dipole moment surface (DMS) was used for the calculation of line intensities and reproduces high-precision experimental intensity data with an accuracy close to 1%. The final line list uses empirical energy levels whenever they are available, to ensure that line positions are reproduced as accurately as possible. The POKAZATEL line list contains over 5 billion transitions and is available from the ExoMol website (www.exomol.com) and the CDS database.

Key words: molecular data opacity planets and satellites: atmospheres stars: atmospheres stars: low-mass - stars: brown dwarfs. astronomical data bases: miscellaneous.

1 INTRODUCTION

Water is prevalent in the Universe. In particular, the existence of water in a wide range of hot astronomical environments has led to the computation of very extensive line lists of rotation-vibration transitions both for the main H₂¹⁶O isotopologue (Allard et al. 1994; Viti et al. 1997; Partridge & Schwenke 1997; Barber et al. 2006) as well as for its minor isotopologues (Voronin et al. 2010; Partridge & Schwenke 1997; Shirin et al. 2008; Polyansky et al. 2017). The most widely used water line lists are probably the ones due to Partridge & Schwenke (1997), henceforth referred to as the Ames line list, and to Barber et al. (2006), henceforth BT2. The Ames line list contains approximately 300 million lines while BT2 contains 500 million lines. BT2 provided the main input for water in the 2010 release of the HITEMP database (Rothman et al. 2010); it has since been subject to a number of validations by comparison with laboratory measurements (Bordbar et al. 2014; Alberti et al. 2015; Melin & Sanders 2016). Such comparisons have shown that the Ames line list is often more accurate than BT2 for transitions with wavelengths longer than 1 μm (wavenumbers $< 10\,000\text{ cm}^{-1}$) but drops in accuracy at shorter wavelengths. By virtue of its greater number of lines, BT2 gives an excellent coverage for high temperatures up to 3000 K but it is missing significant flux at higher temperatures and for shorter wavelengths. Thus none of these line lists can be considered to be fully satisfactory.

The BT2 line list has been used as the basis for a number of atmospheric models such as the widely used BT-Settl model of Allard (2014). However, there is increasing evidence of the presence of water on objects hotter than 3000 K, in which case the coverage offered by BT2 is inadequate. For example, water has been observed at an effective temperature of over 4000 K

* Email: j.tennyson@ucl.ac.uk

in sunspots (Sonnabend et al. 2006) and in a variety of giant stars with temperatures between 3500 and 5000 K (Jennings & Sada 1998; Tsuji 2001; Ryde et al. 2006; Abia et al. 2012; Ryde et al. 2015), on dwarf stars with temperatures up to 4000 K (Rajpurohit et al. 2014) and on variable stars whose atmospheres can also reach these temperatures (Banerjee et al. 2005; Pavlenko et al. 2008).

At slightly lower temperatures, water was the first molecule to be observed in exoplanetary atmospheres (Tinetti et al. 2007) and it is now known to be a common constituent of hot Jupiters (Beaulieu et al. 2010; Iyer et al. 2016) and other exoplanets (Fraine et al. 2014). Some of these exoplanet observations require high accuracy laboratory data (Birkby et al. 2013; Brogi et al. 2014).

Apart from modelling hot objects, transitions involving highly excited energy levels may be important in environments far from thermodynamic equilibrium; for example, water fluorescence on comets can occur from very highly excited levels (Dello Russo et al. 2004, 2005; Barber et al. 2007); such observations are not always well-understood (Barber et al. 2007). Similarly observations with the Atacama Large Millimeter Array (ALMA) are beginning to probe maser emission from vibrationally excited water (Hirota et al. 2012, 2016); modelling water maser emission requires very extensive transition datasets (Gray et al. 2016). Finally, extensive water line lists are also important for many terrestrial applications, such as modelling and monitoring of emissions from combustion engines (Kranendonk et al. 2007; Rein & Sanders 2010) or studying high-explosive blast waves (Carney et al. 2011).

There have been a number of important developments since the computation of the Ames and the BT2 line lists, which suggests that we now in a position to compute an H_2^{16}O line list which is both more comprehensive, indeed effectively complete, and more accurate than either of these. In particular, improved theoretical methods have led to the development of both potential energy surfaces (PES) (Barletta et al. 2006; Lamouroux et al. 2008; Lodi & Tennyson 2008; Bubukina et al. 2011; Shirin et al. 2006; Császár et al. 2010; Polyansky et al. 2013; Mizus et al. 2018) and dipole moment surfaces (DMS) (Lamouroux et al. 2008; Lodi et al. 2008, 2011) with significantly improved accuracy, and nuclear motion calculations which extend all the way to dissociation (Mussa & Tennyson 1998; Li & Guo 2001; Császár et al. 2010). Indeed, our ability to compute high-accuracy transition intensities is leading to such computations (Pavanello et al. 2012; Kyuberis et al. 2017; Birk et al. 2017) replacing measurements in standard compilations such as HITRAN (Gordon & et al. 2017). In addition work by an IUPAC (International Union of Pure and Applied Chemistry) task group (Tennyson et al. 2009, 2010, 2013, 2014a, 2014b) has led to the determination of accurate experimental water energy levels; such very accurate, experimentally derived energy levels can be used to replace computed ones, resulting in both near-perfect reproduction of laboratory transition frequencies and in the prediction of many unobserved line positions with similar accuracy.

In this work we exploit these advances to produce a new line list for the main water isotopologue H_2^{16}O . This work is performed as part of the ExoMol project (Tennyson & Yurchenko 2012), which aims to provide molecular line lists for exoplanet and other hot atmospheres. A unique feature of the resulting line list, which we call POKAZATEL, is that it is not simply complete up to some given temperature as is usual for ExoMol line lists of polyatomic systems (Tennyson & Yurchenko 2018). Instead, the aim is to capture *all* bound-to-bound transitions in the system, which implies considering all energy levels lying below the dissociation limit. POKAZATEL is thus the first complete rotation-vibrational line list for a polyatomic molecule. Besides covering all temperatures for which the water molecule exists, completeness significantly extends the wavelength range of the line list. In this context, we note the recent detection of near ultra-violet water absorptions in the Earth's atmosphere by Lampel et al. (2017).

Our ability to calculate an accurate and complete water line list is based on the five following factors: (i) the availability of spectroscopically accurate *ab initio* potential energy surface (PES) describing energies up to the lowest dissociation pathway (Polyansky et al. 2013; Császár et al. 2010); (ii) the ability to fit this *ab initio* PES to empirical energy levels, which significantly improves the accuracy of computed line positions; (iii) an efficient programme suite, DVR3D (Tennyson et al. 2004; Tennyson & Yurchenko 2017), which allows us to compute accurate energies, wavefunctions, dipole moment integrals and intensities of transitions up to dissociation; (iv) availability of spectroscopic data covering not only the conventional infrared and optical regions below $26\,000\text{ cm}^{-1}$ (Tolchenov et al. 2005; Polyansky et al. 1998, 1997; Schermaul et al. 2002) but also multiphoton spectra probing the region up to (Grechko et al. 2009) and even exceeding (Zobov et al. 2011) dissociation; such experimental input allowed us to accurately characterise our new water PES up to dissociation; (v) progress in computer hardware, especially in terms of storage, allowed us to undertake comprehensive computations previously impractical; for example, nuclear-motion wavefunctions relative to a single value of the J angular momentum often occupy more than 1 Tb of storage.

This paper is organized as follows. In section II we describe the PES used in this work. Section III presents details on line position and line intensity calculations. In section IV we compare our calculated energy levels with experimental values and with existing line lists. Section V presents the POKAZATEL line list and discusses some ways of using it for modelling water spectra. Section VI concludes the paper.

2 CALCULATION OF THE PES

The major, distinguishing feature of POKAZATEL with respect to its predecessors (Partridge & Schwenke 1997; Viti et al. 1997; Barber et al. 2006) is its completeness in both vibrational and rotational states. The $J = 0$ vibrational energy levels included in POKAZATEL reach energies of 40000 cm^{-1} , just below the H_2^{16}O dissociation energy $D_0 = 41\,146.1 \text{ cm}^{-1}$ (Boyarkin et al. 2013). To ensure completeness in rotational levels we determined the highest J for which the lowest rotational energy of the ground vibrational state is below $41\,000 \text{ cm}^{-1}$. This J turns out to be $J = 72$. In other words, for $J = 73$ all the levels lie above $41\,000 \text{ cm}^{-1}$ and were not considered. The inclusion of metastable levels beyond dissociation is, in principle, also possible but would require a significant extension of the methodology employed in this work. Besides, such transitions are likely to be important only at temperatures at which water is effectively decomposed and so they are not expected to contribute significantly to the molecular opacity.

In order to calculate energy levels up to $41\,000 \text{ cm}^{-1}$ accurately we require two things. First, a computer program for solving the rotation-vibrational Schrödinger equation capable of computing all the required states to the necessary accuracy. Second, we need an accurate PES capable of reproducing to high accuracy (to approximately 0.05 cm^{-1}) experimentally known energy levels and covering all energies up to dissociation. The DVR3D program of Tennyson et al. (2004) satisfies our first requirement and has recently benefitted from a number of algorithmic improvements as part of the ExoMol project (Azzam et al. 2016; Underwood et al. 2016; Tennyson & Yurchenko 2017) which proved vital for completing the necessary calculations.

A water PES fulfilling our second requirement was not available, so we produced one as part of this work. Our previous, spectroscopically determined water PESs (Polyansky et al. 1996; Shirin et al. 2003; Bubukina et al. 2011) combined with new *ab initio* calculations of the H_2O PES provided us with a very good starting point for constructing our new PES. However, even with these surfaces available, it was not easy to produce a PES which both extends up to dissociation and provides near-spectroscopic accuracy. Our fitted PES is based on two separate datasets of water energy levels. The first set consists of conventional spectroscopic data up to $25\,000 \text{ cm}^{-1}$, also used in our previously fits (Shirin et al. 2003; Bubukina et al. 2011); the second set comprises energy levels from $27\,000 \text{ cm}^{-1}$ up to D_0 obtained using two-photon and three-photon action spectroscopy (Maksyutenko et al. 2007; Grechko et al. 2008, 2009).

Initially, we tried to produce a single PES reproducing the data belonging to both sets; this proved to be impossible, as any attempt to reproduce the high-lying energy levels to better than 1 cm^{-1} resulted in an unacceptable deterioration in low-energy levels. Eventually we decided to follow Varandas (1996) and use two separate PES representations joined by a switching function:

$$V_{\text{glob}} = V_{\text{low}}f(E) + V_{\text{up}}(1 - f(E)), \quad (1)$$

$$f = 0.5[1 + \tanh(\gamma\Delta E)]$$

$$\gamma = \gamma_0 + \gamma_1\Delta E^2$$

$$\Delta E = V_u - E_0$$

$$\gamma_0 = 1/500, \gamma_1 = 1/500^3, E_0 = 35000 \quad (2)$$

where the values for the constants are appropriate for energies in wavenumbers.

The upper and lower surfaces employ the same functional form but have different coefficients

$$V(S_1, S_2, S_3) = V_0 + \left[\sum_{i,j,k} f_{ijk} S_1^i S_2^j S_3^k \right] x_3 + V_{\text{HH}} + x_1 + x_2 \quad (3)$$

$$x_1 = D[\exp(-2\alpha\Delta r_1) - 2\exp(-\alpha\Delta r_1)] + D$$

$$x_2 = D[\exp(-2\alpha\Delta r_2) - 2\exp(-\alpha\Delta r_2)] + D$$

$$x_3 = \exp[-b_1(\Delta r_1^2 + \Delta r_2^2)]$$

$$V_{\text{HH}} = 82000 \exp(-6.2r_{\text{HH}}) \quad (4)$$

$$S_1 = (r_1 + r_2)/2 - r_e, S_2 = (r_1 - r_2)/2, S_3 = \cos\theta - \cos\theta_e, \Delta r_i = r_i - r_e \quad (5)$$

where units of Å and cm^{-1} are used throughout. r_1 , r_2 and θ are the standard bond lengths and bond angle of water, and $r_e = 0.9586 \text{ Å}$ and $\theta_e = 104.48^\circ$ are fixed to reference equilibrium values (Császár et al. 2005). The functions x_1 and x_2 are Morse potentials for each of the OH bonds, x_3 is a damping function and the term V_{HH} is a function of r_{HH} representing the distance between the H atoms and is introduced to avoid artificial minima in the region where the H atoms are close to each

other (Choi & Light 1992). Other non-linear constants were fixed as follows: $b_1 = 2.15 \text{ \AA}^{-1}$, $D = 43900 \text{ cm}^{-1}$, $\alpha = 2.2668 \text{ \AA}^{-1}$. The coefficients f_{ijk} were determined as discussed below.

The switch between two potentials ($E_0 = 35\,000 \text{ cm}^{-1}$) was chosen significantly above $26\,000 \text{ cm}^{-1}$ to minimize the influence of the upper PES, V_{up} , on low-lying levels. The starting point for V_{low} was the potential of Bubukina et al. (2011), while the starting point for V_{up} was the *ab initio* PES by Császár et al. (2010). V_{low} was then determined using a fitting procedure similar to the one employed by Bubukina et al. (2011) for the levels below $26\,000 \text{ cm}^{-1}$; in this region a set of 1562 empirical energy levels with $J = 0, 2, 5$ was used.

For the fit for V_{up} we took as starting point the *ab initio* surface Császár et al. (2010) and then performed a fit of 734 levels with $J = 0, 2$ up to $41\,000 \text{ cm}^{-1}$. Of the 41 known $J = 0$ empirical levels above $27\,000 \text{ cm}^{-1}$, 15 levels had to be excluded from the fit. For $J = 2$ levels about 25 % of the high-lying levels were excluded. Low-energy levels below $27\,000 \text{ cm}^{-1}$ were also included in the fit but they were assigned a weight 5 to 10 times lower than high-energy ones.

All fits used the approach of Yurchenko et al. (2003), in which the fitted potential energy surface is partially constrained by a set of reference *ab initio* data in order to prevent the emergence of nonphysical behaviour such as artificial peaks or troughs. Specifically, the following functional was minimised:

$$F = \sum_i (E_i^{(\text{obs})} - E_i^{(\text{calc})})^2 w_i^{\text{en}} + d \sum_k (V_k^{(\text{abinitio})} - V_k^{(\text{calc})})^2 w_k^{\text{PES}}, \quad (6)$$

where E_i are the ro-vibrational energy term values, V_k represents the value of the *ab initio* PES at the k -th geometry, w_i are the corresponding weight factors for the individual energies/geometries normalized to one and d is a further factor defining the relative importance of the *ab initio* PES relative to the experimental energies. A total of 1460 *ab initio* points were chosen for this constraint, covering the energy region up to about $50\,000 \text{ cm}^{-1}$, which corresponds to O–H bond lengths and H–O–H interbond angles ranging from 0.65 to 2.7 \AA and from 35° to 177° , respectively. The final PES was found to deviate from the *ab initio* set of points by less than 40 cm^{-1} for all geometries, which indicates that it preserves a physically correct behaviour also for geometries uncharacterised by the available experimental energy levels.

The weights in Eq. (6) are normalized as follows:

$$\sum_i w_i^{\text{en}} + \sum_k d w_k^{\text{PES}} = 1. \quad (7)$$

The minimum of the function F was then found using a simple steepest decent algorithm by simultaneously fitting the potential parameters both to the experimental energies and to *ab initio* points (Yurchenko et al. 2003). The required derivatives of the energies with respect to the potential parameters were computed using the Hellmann-Feynman theorem. In our analytical representation the potential parameters are included linearly, which simplifies the evaluation of the integrals:

$$\frac{\partial E_n}{\partial f_{ijk}} = \langle \psi_n | \frac{\partial \Delta V}{\partial f_{ijk}} | \psi_n \rangle = \langle \psi_n | S_1^i S_2^j S_3^k x_3 | \psi_n \rangle. \quad (8)$$

where E_n and ψ_n are the eigenvalues and eigenfunctions of the ro-vibrational Hamiltonian H , respectively, n is a running index, and the f_{ijk} are the coefficients of PES expansion.

For the fits we used the fitting wrapper `DVR3D_SFit` (simultaneous fit) written for DVR3D and also used by Bubukina et al. (2011). This is a Fortran 95 program which automatically calls the necessary programs from the DVR3D suite, namely `DVR3DRJZ`, `Rotlev3B`, and `Xpect3`. This method was used also to refine an H_2S *ab initio* PES by Azzam et al. (2016). The wrapper can be downloaded from CCPForge (www.ccpforge.cse.rl.ac.uk) as part of the DVR3D project.

Initially, before performing any fit, our initial, composite PES gave observed minus calculated (obs–calc) residues of about 0.1 cm^{-1} for levels below $25\,000 \text{ cm}^{-1}$. We then re-fitted V_{low} using the lower levels while keeping V_{up} constant. This led to these levels being reproduced with a standard deviation, σ , of 0.04 cm^{-1} . After this, the upper part of the potential V_{up} was fitted using the levels between $25\,000$ and $41\,000 \text{ cm}^{-1}$. This final fit gave $\sigma = 0.13 \text{ cm}^{-1}$ for all levels and $\sigma = 0.04 \text{ cm}^{-1}$ for the levels below $26\,000 \text{ cm}^{-1}$.

To improve the accuracy of the calculated energy levels at high angular momentum J_s we used rotational nonadiabatic correction based on those of Schwenke (2001). Specifically, we used additional operators J_{xx} , J_{yy} , and J_{zz} to take into account the influence of nonadiabatic effects on highly excited rotational states. The coefficients in front of these operators were treated as additional adjustable parameters and were optimized in calculations of the energy levels with rotational quantum number $J = 20$; this optimization fixed their values at 0.194 , 0.194 , and 0.14 , respectively.

The final potential contains two sets of 246 constants and is given in the supplementary material as a Fortran program. Section IV below gives a comparison between energy levels computed using the PES V_{glob} of Eq. (1) with both experimentally derived ones and with previous calculations.

3 NUCLEAR MOTION CALCULATIONS

The PES described in the previous section was used to calculate energy levels up to the energy of $40\,000 \text{ cm}^{-1}$ and for angular momentum up to $J = 72$. The programs `DVR3DRJZ` and `Rotlev3B` from the DVR3D program suite (Tennyson et al. 2004)

were used to perform the nuclear motion calculations. The energy levels and corresponding wavefunctions were then used to calculate dipole matrix elements using the program Dipole3. In turn, these matrix elements were then used in the program Spectra (Tennyson et al. 1993) to calculate the line positions and intensities for water transitions in the region from 0 to 40 000 cm^{-1} . Nuclear masses were used in all calculations.

The DVR3DRJZ calculations used Radau coordinates with 60 radial grid points and 40 angular grid points. The radial coordinates were represented using Morse-like oscillators with parameters $r_e = 3.0$, $D_e = 0.25$, $\omega_e = 0.007$ in atomic units; associated Legendre polynomials were used for the angular coordinate. Final vibrational matrices dimension of 5500 were diagonalised to give basis functions for the full rotation-vibration calculation. For the rotational problem, the dimensions of final matrices fixed at $400(J + 1 - p)$, where J is the total angular momentum quantum number and p is the value of parity. Our final energy levels are converged to better than 0.1 cm^{-1} at energies around 40 000 cm^{-1} , and significantly better than this below 40 000 cm^{-1} .

4 RESULTS OF THE ENERGY LEVELS CALCULATIONS

To illustrate the accuracy of the energy levels associated with the line list calculations, we compare computed energy levels with a representative sample of experimentally derived ones for H_2O . Of particular significance is the comparison of $J = 0$ vibrational term values, as usually discrepancies between observed and calculated (obs–calc) energy levels for any J can be decomposed in a major J -independent vibrational contribution and in a much smaller J -dependent rotational one (Polyansky et al. 1997). Table I gives a comparisons for all experimentally known vibrational term values. These data are representative of the general accuracy of all levels.

From Table I we can draw the following conclusions. First, the POKAZATEL vibrational energy levels up to 18 000 cm^{-1} are more accurate than the ones of previous line lists (Partridge & Schwenke 1997; Shirin et al. 2003). Levels marked with stars were not used in the fit of Partridge & Schwenke (1997) as they were experimentally unknown at that time and show the largest differences with experiment in that line list. In particular, un-starred levels below 16 000 cm^{-1} are reproduced in the PS line list with a root-mean-square (RMS) deviation of 0.06 cm^{-1} , while the deviation for starred levels is 0.41 cm^{-1} for levels up to 20 000 cm^{-1} (beyond this energy the PS line list quickly becomes completely unreliable). Note that the (un-starred) levels included in the fit of Partridge & Schwenke (1997) are reproduced better by both POKAZATEL and Bubukina et al. (2011) with a deviation of, respectively, 0.03 cm^{-1} and 0.01 cm^{-1} , while BT2 is comparable with PS with a mean average deviation for those levels of 0.08 cm^{-1} . Overall levels below 25 000 cm^{-1} are best reproduced by the PES of Bubukina et al. (2011), although POKAZATEL follows very closely.

In the energy range between 18 000 and 30 000 cm^{-1} one finds discrepancies of up to 10 cm^{-1} for Partridge & Schwenke (1997) and up to 5 cm^{-1} for the BT2 line lists, which used a PES by Shirin et al. (2003). The largest improvement of POKAZATEL with respect to previous line lists is for energies approaching 40 000 cm^{-1} , for which, Partridge & Schwenke (1997) gives discrepancies of up to 300 cm^{-1} while our new line lists give about 0.1 cm^{-1} for levels included in the fit and about 1 cm^{-1} for levels not included in the fit. Of course, Partridge & Schwenke (1997) did not attempt to fit this region and these results simply illustrate the well-known unreliability of extrapolation of spectroscopically determined PESs.

Another way to present the comparisons between calculated and experimental values is standard deviations for separate J s. This gives more details than overall standard deviation for all the levels and is presented in the Table II.

In Table II we report rms deviations for energy levels of given rotational angular momentum J relative to the PES by Bubukina et al. (2011) and to our new POKAZATEL one. One can see that for POKAZATEL energy levels up to 25 000 cm^{-1} the deviations with respect to experiment grow with J , going from about 0.04 cm^{-1} for $J = 0-5$ to about 0.2 cm^{-1} for $J = 35-40$. For the levels up to 41 000 cm^{-1} , which are only known for the $J \leq 7$, deviations are somewhat larger - up to 0.1 cm^{-1} .

The PES by Bubukina et al. (2011), which extends only up to 26 000 cm^{-1} , gives deviations which are about half than the ones from POKAZATEL for energy levels below 25 000 cm^{-1} .

For intensity calculations wavefunctions obtained with the POKAZATEL PES were used in all cases. However, for our final set of energy levels given in the states file (see below) the following strategy was used. Where available, empirical energies obtained using the MARVEL procedure by the IUPAC task group (Tennyson et al. 2013) are used. Transitions between these levels should give line positions with experimental accuracy even when these are yet to be observed. Unknown energy levels below 18 000 cm^{-1} and with $J \leq 50$ were generated using the PES of Bubukina *et al.* as these better reproduce observed line positions in this low-energy range. Otherwise levels from the POKAZATEL PES are used. This strategy gives the best available estimate for each energy level; our data structure allows the states file to be further updated in the eventuality that better (empirical) energies become available in the future (see, for example, Barber et al. (2014)).

Table 1: Comparison of calculated and experimentally derived (Tennyson et al. 2013) vibrational term values in cm^{-1} for H_2^{16}O for four different PESs: POKAZATEL (this work), BT2 (Barber et al. 2006), Bubukina (Bubukina et al. 2011) and PS (Partridge & Schwenke 1997); levels marked with a star were not included by PS in their fit. For computed energy levels we report the difference (observed – calculated).

v_1	v_2	v_3	Obs.	obs. – calc.				
				POKAZATEL	BT2	Bubukina	PS	
0	1	0	1594.746	0.020	-0.13	-0.016	-0.03	
0	2	0	3151.630	0.039	-0.05	-0.004	0.00	
1	0	0	3657.053	0.004	-0.10	0.038	0.01	
0	0	1	3755.929	-0.006	0.01	-0.003	-0.03	
0	3	0	4666.790	0.041	0.07	0.000	0.00	
1	1	0	5234.976	0.021	-0.24	0.012	-0.05	
0	1	1	5331.267	0.006	-0.01	-0.002	0.05	
0	4	0	6134.015	0.025	0.18	-0.007	-0.02	
1	2	0	6775.094	-0.013	-0.15	0.011	-0.01	
0	2	1	6871.520	0.011	-0.01	0.011	0.02	
2	0	0	7201.540	-0.011	0.01	0.003	-0.01	
1	0	1	7249.817	-0.066	-0.04	-0.004	-0.04	
0	0	2	7445.056	0.003	-0.04	0.023	-0.06	
0	5	0	7542.372	-0.009	0.16	0.024	-0.14	*
1	3	0	8273.976	-0.018	-0.12	-0.001	-0.07	
0	3	1	8373.851	0.003	0.00	0.011	-0.05	
2	1	0	8761.582	-0.004	-0.12	-0.004	-0.08	
1	1	1	8806.999	-0.040	-0.10	-0.004	-0.04	
0	6	0	8869.950	-0.162	-0.32	-0.212	-0.64	*
0	1	2	9000.136	0.000	-0.02	0.017	0.03	
0	4	1	9833.583	-0.008	0.08	0.004	-0.05	
2	2	0	10284.364	-0.025	0.01	0.000	0.01	
1	2	1	10328.729	-0.047	0.03	0.001	0.06	
0	2	2	10521.758	-0.017	-0.05	0.031	-0.01	*
3	0	0	10599.686	-0.025	0.09	-0.003	0.01	
2	0	1	10613.356	-0.076	-0.03	-0.003	-0.04	
1	0	2	10868.875	-0.022	0.03	0.005	-0.02	
0	0	3	11032.404	-0.050	-0.05	0.016	-0.06	
0	5	1	11242.776	-0.008	0.16	0.002	0.00	*
2	3	0	11767.389	-0.008	-0.09	0.004	-0.13	*
1	3	1	11813.207	-0.034	0.00	-0.007	-0.02	
0	3	2	12007.774	-0.043	-0.14	0.011	-0.15	*
3	1	0	12139.315	-0.031	-0.01	0.003	-0.04	
2	1	1	12151.254	-0.057	-0.10	0.010	-0.07	
1	1	2	12407.662	-0.016	0.00	0.010	0.01	
0	1	3	12565.006	-0.043	-0.02	0.010	0.00	
3	2	0	13640.717	-0.023	0.25	0.077	0.14	*
2	2	1	13652.655	-0.033	0.21	0.021	0.19	
4	0	0	13828.275	-0.001	-0.01	0.013	0.11	
3	0	1	13830.938	-0.034	-0.07	0.001	0.10	
0	7	1	13835.373	0.035	-0.52	-0.022	-0.48	*
1	2	2	13910.894	-0.036	0.08	0.013	0.10	
0	2	3	14066.194	-0.056	0.01	0.014	-0.02	
2	0	2	14221.159	-0.024	0.10	0.004	0.03	
1	0	3	14318.813	-0.053	-0.01	0.010	0.06	
1	5	1	14647.971	-0.066	-0.17	0.002	-0.22	*

2	3	1	15119.028	-0.008	0.02	0.014	0.00		
4	1	0	15344.503	-0.012	-0.09	0.005	0.09		
3	1	1	15347.956	-0.035	-0.10	0.001	0.11		
0	3	3	15534.709	-0.050	-0.06	0.008	-0.12	*	
2	1	2	15742.797	-0.062	-0.01	-0.021	0.01		
1	1	3	15832.766	-0.053	0.00	0.016	0.09		
2	4	1	16546.319	-0.010	-0.10	0.017	-0.12	*	
3	2	1	16821.631	0.007	0.39	-0.000	0.54	*	
4	2	0	16823.319	0.031	0.20	0.024	0.35	*	
4	0	1	16898.842	0.000	0.31	0.001	0.56	*	
2	2	2	17227.380	0.034	0.14	0.051	0.26	*	
1	2	3	17312.551	-0.077	0.25	0.005	0.31	*	
3	0	2	17458.213	0.060	0.08	0.014	0.29	*	
2	0	3	17495.528	-0.038	-0.07	0.033	0.27	*	
1	0	4	17748.107	-0.032	-0.22	0.010	0.14	*	
3	3	1	18265.821	-0.031	0.04	-0.008	0.12	*	
5	1	0	18392.778	0.021	0.08	-0.008	0.84	*	
4	1	1	18393.315	0.003	0.10	-0.015	0.84	*	
1	3	3	18758.636	-0.055	0.04	0.018	0.17	*	
2	1	3	18989.960	-0.038	-0.06	0.019	0.30	*	
5	0	1	19781.103	0.009	-0.20	0.002	1.06	*	
6	0	0	19781.323	0.028	-0.69	0.013	0.73	*	
4	2	1	19865.285	0.011	0.74	0.014	1.79	*	
2	2	3	20442.777	-0.011	0.29	0.031			
3	0	3	20543.129	-0.024	-0.14	0.034			
5	1	1	21221.827	-0.038	-0.52	0.024			
4	3	1	21314.448	0.040	1.14	0.055			
7	0	0	22529.295	-0.054	0.06	-0.005	2.51	*	
6	0	1	22529.441	-0.054	0.08	0.004	2.50	*	
7	0	1	25120.278	-0.067	0.52	0.015	4.25	*	
5	3	2	27502.660	-0.232	-0.85				
9	0	0	27540.690	0.148	1.11		4.23	*	
6	1	2	27574.910	-0.069	0.50				
9	1	0	28934.140	0.833	3.20				
10	0	0	29810.850	0.417			7.30	*	
8	0	2	31071.570	-0.034					
10	1	0	31207.090	-1.724					
11	0	0	31909.679	0.673			9.14	*	
11	1	0	33144.709	-0.080					
11	0	1	33835.222	0.164			15.33	*	
12	0	0	33835.249	0.193			15.36	*	
13	0	0	35585.957	0.407			44.65	*	
12	0	1	35586.007	-0.565			43.14	*	
12	2	0	36179.317	-5.567					
13	1	0	36684.047	-2.843					
12	1	1	36684.877	-2.052					
9	1	3	36739.777	-2.312					
10	1	2	36740.597	-1.841					
14	0	0	37122.697	0.517			108.47	*	
13	0	1	37122.717	0.556			108.50	*	
11	3	1	37309.847	0.221					
12	3	0	37311.277	-0.593					
13	2	0	37765.647	0.186					
14	1	0	38153.247	0.029					
13	1	1	38153.307	0.045					
15	0	0	38462.517	1.094			283.17	*	
14	0	1	38462.537	1.112			283.11	*	

14	2	0	39123.767	0.240
14	1	1	39390.217	1.220
15	1	0	39390.257	1.258
15	0	1	39574.537	0.249
16	0	0	39574.547	0.218
12	1	2	40044.567	-3.005
11	1	3	40044.671	2.611
14	2	1	40226.261	-4.185
13	3	1	40262.001	-5.579
16	1	0	40370.547	-0.921
15	1	1	40370.781	-0.764
16	0	1	40437.211	1.941
12	0	3	40704.156	-2.329
17	0	1	40945.693	0.270
18	0	1	41100.053	1.468
19	0	0	41101.337	-0.554
15	2	1	41121.606	4.564

Our nuclear-motion calculations assign to energy levels only exact quantum numbers, namely J , parity and the ortho/para symmetry label. Furthermore, energy levels within a given J -parity-symmetry subset are labelled in increasing order of energy with a counting index i .

However, it is convenient and standard practice to label energy levels with approximate (normal mode) vibrational $\nu_1\nu_2\nu_3$ and (rigid rotor) rotational JK_aK_c quantum numbers. Assigning such labels to every level up to dissociation is difficult (Császár et al. 2010) and probably formally impossible (Child et al. 1999). Nevertheless, many energy levels can indeed be successfully labelled and such labelling is useful in some applications, e.g. when considering pressure broadening. For low v and J the labelling procedure is straightforward while for higher excitations a variety of methods were used, which will be discussed elsewhere. In our line list vibrational ($\nu_1\nu_2\nu_3$) and rotational (JK_aK_c) labels were assigned to more than 72 000 H₂O energy levels with energies up to 20 000 cm⁻¹ and $J \leq 28$.

5 CALCULATION AND REPRESENTATION OF THE LINE LIST

The program suite DVR3D calculates the bound rotation-vibration energy levels and the corresponding wavefunctions on a three dimensional grid. Using these wavefunctions and the LTP2011S DMS (Lodi et al. 2011) we computed the Einstein A coefficients, A_{if} , for transitions up to $J = 72$ and the energies up to 40 000 cm⁻¹.

The ExoMol database uses a condensed format which separates transitions into a states file (which includes quantum labels where available) and a transitions file (Tennyson et al. 2013). Extracts from these two files are given in Tables 3 and 4, respectively. These files, which contain 810 269 states and 5 745 071 340 transitions can be obtained from `ftp://cdsarc.u-strasbg.fr/pub/cats/J/MNRAS/xxx/yy`, or `http://cdsarc.u-strasbg.fr/viz-bin/qcat?J/MNRAS//xxx/yy` as well as the ExoMol website, `www.exomol.com`.

In order to further improve the accuracy of the line positions presented in the POKAZATEL line list, we produced two additional sets of energy levels, presented as two different states files in ExoMol format, which are made available in the supplementary material. In the first additional file we substituted the POKAZATEL energy levels up to 20 000 cm⁻¹ with the ones calculated with the PES by (Bubukina et al. 2011). A comparison between the POKAZATEL PES and the PES by (Bubukina et al. 2011) is reported in Tables 1 and 2 and shows that energy levels produced by (Bubukina et al. 2011) are somewhat more accurate than the ones resulting from POKAZATEL for energies up to about 20 000 cm⁻¹.

A second set of energy levels was produced exclusively from experimentally derived ones. This set of levels is significantly more limited but much more accurate, as its accuracy corresponds to the one of experimental observations.

Using our calculations we also computed the partition function for H₂¹⁶O for wide range of temperatures. The partition function of water is important for a variety of applications and high accuracy studies are available concentrating solely on this quantity (Vidler & Tennyson 2000; Furtenbacher et al. 2016). Table 5 compares our partition function with those from various previous studies. All partition functions are computed using the HITRAN convention (Gamache et al. 2017), adopted by the ExoMol project, which explicitly includes the spin degeneracy of all particles. As the value of the partition function at a given temperature always increases when more energy levels are included in its calculation, such value can be used as a measure of the completeness of a given line list at that temperature (Neale et al. 1996).

Table 5 shows that the POKAZATEL partition function gives excellent agreement with the recent ‘definitive’ partition

Table 2. Comparison of obs–calc root-mean-square deviations (σ) in cm^{-1} as a function of rotational (J) states for calculations using our new POKAZATEL PES and using the PES by Bubukina et al. (2011). The reported rms deviations are relative to energy levels up to E_{max} . N_J is the number of levels considered in each case.

PES= E_{max}	POKAZATEL 26 000 cm^{-1}		Bubukina 25 000 cm^{-1}		POKAZATEL 41 000 cm^{-1}	
	J	σ	N_J	σ	N_J	σ
0	77	0.034	78	0.023	86	0.113
1	274	0.039	270	0.022	306	0.112
2	482	0.040	475	0.032	548	0.112
3	679	0.037	673	0.029	719	0.081
4	841	0.039	842	0.033	875	0.065
5	994	0.047	997	0.031	1025	0.075
6	1064	0.055	1069	0.032	1074	0.064
7	1110	0.070	1104	0.035	1112	0.072
8	1035	0.087	1037	0.037		
9	953	0.109	950	0.039		
10	857	0.125	851	0.044		
11	750	0.134	752	0.054		
12	676	0.150	672	0.063		
13	615	0.157	605	0.069		
14	575	0.169	560	0.075		
15	527	0.179	519	0.082		
16	494	0.183	503	0.097		
17	474	0.193	480	0.108		
18	450	0.194	460	0.116		
19	442	0.206	450	0.124		
20	432	0.210	420	0.126		
21	399	0.203	396	0.131		
22	366	0.209	358	0.134		
23	344	0.212	329	0.138		
24	316	0.219	306	0.140		
25	283	0.207	268	0.142		
26	251	0.193	234	0.154		
27	238	0.189	228	0.162		
28	218	0.185	193	0.163		
29	181	0.194	172	0.163		
30	143	0.190	124	0.165		
31	110	0.198				
32	81	0.185				
33	46	0.213				
34	24	0.223				
35	19	0.198				
36	17	0.217				
37	11	0.199				
38	10	0.170				
39	4	0.186				

function of Furtenbacher et al. (2016). The agreement between these and the older partition function of Vidler & Tennyson (2000) is also excellent; Vidler & Tennyson also considered all states up to dissociation with $J \leq 72$ but used a rather crude model for the high-lying energies. This illustrates an important point: for accurate partition sums at high temperatures completeness of the energy level list is more important than accuracy of individual levels. Conversely, both the BT2 and the Ames partition sums are too low at high temperatures, which reflects the incompleteness of these line lists. Our partition function is given in the supplementary data on a grid of 1 K.

To illustrate our results Fig. 1 and 2 present plots of H_2O spectra in various spectral regions and for various temperatures. Below about 2500 K, at the low resolution of the plots POKAZATEL coincides quite closely with BT2 for wavenumbers up to 25 000 cm^{-1} .

BT2 uses an energy limit of 30 000 cm^{-1} and was designed to be complete for transitions below 20 000 cm^{-1} and, as a result, its predictions are very different from the ones by POKAZATEL in the near-UV region above 25 000 cm^{-1} , see fig. 1. In particular, the BT2 line list predicts a much larger absorption in the near-UV region than POKAZATEL. The quality of the POKAZATEL line list in this region has been demonstrated in recent analysis of ultraviolet terrestrial atmospheric absorption (Lampel et al. 2017), so we can conclusively say that BT2 overestimates absorption in this region.

At room temperature and for visible wavelengths POKAZATEL and the recent release of HITRAN (Gordon & et al. 2017) give reasonable agreement, but HITRAN contains no data on near-ultraviolet transitions. At high temperatures, as

Table 3. Extracts from the final states file for the POKAZATEL line list showing portions with full quantum number assignments (upper part) and only rigorous quantum numbers given (lower part).

i	\tilde{E}	g_{tot}	J	K_a	K_c	ν_1	ν_2	ν_3	S
2	1594.746306	1	0	0	0	0	1	0	A1
3	3151.629850	1	0	0	0	0	2	0	A1
4	3657.053255	1	0	0	0	1	0	0	A1
5	4666.790461	1	0	0	0	0	3	0	A1
6	5234.975555	1	0	0	0	1	1	0	A1
7	6134.015008	1	0	0	0	0	4	0	A1
8	6775.093508	1	0	0	0	1	2	0	A1
9	7201.539855	1	0	0	0	2	0	0	A1
10	7445.056211	1	0	0	0	0	0	2	A1
11	7542.372492	1	0	0	0	0	5	0	A1
12	8273.975695	1	0	0	0	1	3	0	A1
13	8761.581581	1	0	0	0	2	1	0	A1
14	8869.950054	1	0	0	0	0	6	0	A1
15	9000.136035	1	0	0	0	0	1	2	A1
16	9724.179914	1	0	0	0	1	4	0	A1
17	10085.961796	1	0	0	0	0	7	0	A1
18	10284.364368	1	0	0	0	2	2	0	A1
19	10521.757715	1	0	0	0	0	2	2	A1
20	10599.685969	1	0	0	0	3	0	0	A1
100	21703.511719	1	0	-2	-2	-2	-2	-2	A1
101	21764.097656	1	0	-2	-2	-2	-2	-2	A1
102	21844.693359	1	0	-2	-2	-2	-2	-2	A1
103	21916.152344	1	0	-2	-2	-2	-2	-2	A1
104	21972.789062	1	0	-2	-2	-2	-2	-2	A1
105	22006.955078	1	0	-2	-2	-2	-2	-2	A1
106	22127.925781	1	0	-2	-2	-2	-2	-2	A1
107	22166.060547	1	0	-2	-2	-2	-2	-2	A1
108	22326.316406	1	0	-2	-2	-2	-2	-2	A1
109	22376.539062	1	0	-2	-2	-2	-2	-2	A1
110	22385.830078	1	0	-2	-2	-2	-2	-2	A1

i : State counting number.

\tilde{E} : State energy in cm^{-1} .

g_{tot} : Total state degeneracy.

J : Total angular momentum.

K_a : Projection of the angular momentum in the prolate symmetric top limit.

K_c : Projection of the angular momentum in the oblate symmetric top limit.

ν_1 : Symmetric stretch quantum number.

ν_2 : Bending quantum number.

ν_3 : Asymmetric stretch quantum number.

S : State symmetry in C_{2v} .

expected, HITRAN significantly underestimates the absorption. We note that in this region HITEMP (Rothman et al. 2010) corresponds to BT2.

Figure 2 shows a comparison between BT2 and POKAZATEL for the high temperature of 4000 K. It can be seen that the absorption spectrum predicted by BT2 is more structured than that of POKAZATEL. The flattening of the spectrum is characteristic of a more complete treatment, including high J states and vibrational hot bands. High temperature ($T > 3000$ K) models relying on BT2 are therefore missing significant opacity.

Figure 3 presents cross sections computed using ExoCross (Yurchenko et al. 2018) for different temperatures using the POKAZATEL line list. This illustrates the change in the absorption spectra with increasing temperature.

6 CONCLUSION

We present in this work a new, very complete water line list, which we call POKAZATEL. The line list includes vibrational and rotational energies up to $40\,000\text{ cm}^{-1}$ and a maximum rotational angular momentum $J = 72$. Our calculations are based on a newly developed PES for water which extends all the way up to the lowest-energy dissociation pathway. The accuracy of computed energy levels is about 0.1 cm^{-1} for all the energies up to dissociation. In the lower energy region up to $25\,000\text{ cm}^{-1}$

Table 4. Extract from the transitions file for POKAZATEL line list.

f	i	A_{fi}
596233	571007	1.9373e-02
725029	732339	1.0832e-02
329530	297534	8.0899e-04
790239	794617	1.8347e-02
221420	214352	2.3773e-02
421277	402418	6.1962e-02
438351	418788	1.2862e-01
472230	500166	2.6986e-04
442671	459574	1.7567e-03
208210	178893	3.1161e-02
380584	398311	5.4103e-03
437709	442656	4.0364e-03
623411	618141	1.3136e-02
41424	44438	6.1976e-04
638780	616418	2.2414e-04
478821	448210	7.2435e-03
92899	71149	1.3900e-03
190855	172844	3.2447e-02
429814	398308	4.1444e-03
78888	100775	3.7271e-05
735537	742327	2.4587e-04

f : Upper state counting number.

i : Lower state counting number.

A_{fi} : Einstein-A coefficient in s^{-1} .

Table 5. Comparison of partition functions: VT (Vidler & Tennyson 2000), definitive (Furtenbacher et al. 2016), BT2 (Barber et al. 2006) and Ames (Partridge & Schwenke 1997).

T(K)	VT	POKAZATEL	definitive	BT2	Ames
100	35.153	35.15320	35.153 12	35.15451	35.15279
300	178.122	178.1210	178.120 6	178.1279	178.1175
500	386.333	386.3309	386.330 0	386.3446	386.3224
800	823.791	823.7822	823.780 1	823.8028	823.7627
1000	1218.319	1 218.276	1218.273	1 218.299	1 218.247
1200	1717.126	1 717.092	1717.087	1 717.114	1 717.052
1500	2713.816	2 713.061	2713.052	2 713.078	2 713.002
1800	4093.180	4 091.037	4091.024	4 091.046	4 090.949
2000	5279.984	5 276.323	5276.309	5 276.322	5 276.186
2500	9465.976	9 456.146	9456.14	9 455.912	9 455.016
3000	15981.08	15 961.28	15961.3	15 956.96	15 949.21
3200	19433.68	19 408.59	19408.7	19 397.33	19 380.95
3400	23467.56	23 436.15	23436.4	23 409.67	23 377.37
3500	25725.04	25 690.04	25690.4	25 650.77	25 606.48
3600	28155.76	28 116.74	28117.2	28 059.71	27 999.90
3800	33577.48	33 529.18	33530.1	33 415.36	33 310.73
4000	39818.16	39 758.33	39760	39 545.59	39 371.57
4200	46969.6	46 895.09	46899	46 519.39	46 242.48
4400	55128.8	55 036.08	55045	54 404.58	53 980.91
4500	59618.4	59 514.84	59527	58 709.55	58 192.42
4600	64399.2	64 283.29	64300	63 266.73	62 640.65
4800	74888.4	74 743.42	74775	73 168.15	72 271.03
5000	86709.2	86 527.25	86584	84 166.99	82 916.31
5200	99976.4	99 748.69	99847	96 316.52	94 615.14
5400	114808.8	114 523.9	114687	109 664.5	107 400.3
5500	122848.8	122 530.8	122739	116 801.3	114 208.9
5600	131324.8	130 970.1	131234	124 252.9	121 298.7
5800	149644.8	149 204.9	149619	140 117.5	136 330.8
6000	169887.2	169 344.6	169977	157 287.6	152 511.6

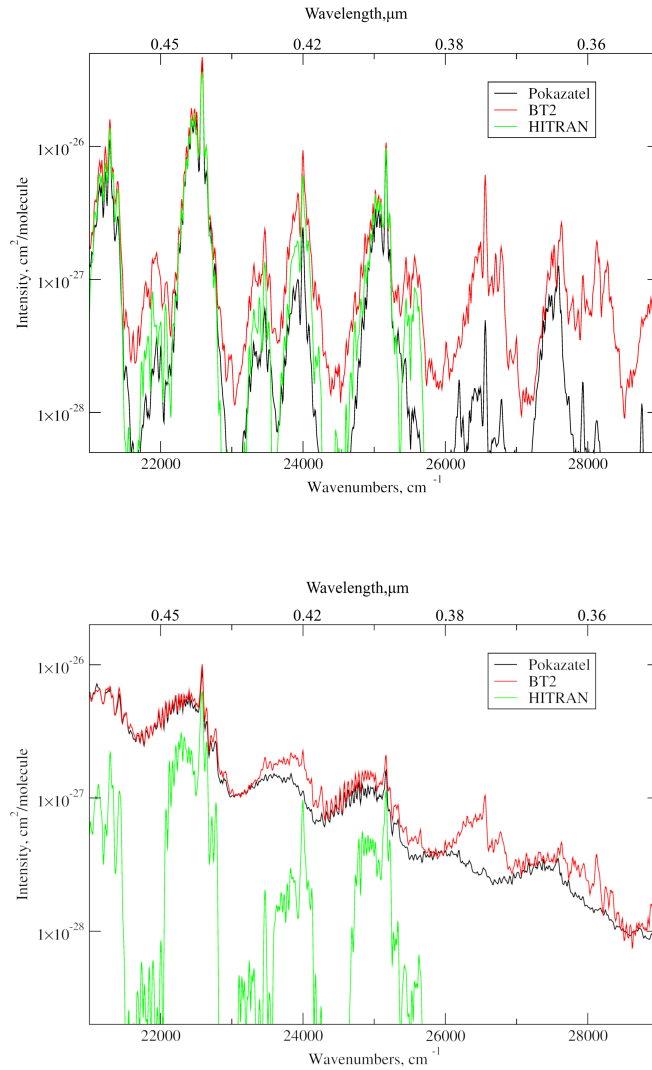


Figure 1. Comparison of BT2 (Barber et al. 2006), POKAZATEL and HITRAN 2016 (Gordon & et al. 2017) at blue and near-ultraviolet wavelengths. Upper plot is for room temperature ($T= 296$ K), lower plot is for $T = 2000$ K.

accuracy is better. The line list comprises nearly 6 billion lines, an order of magnitude more than any previous line list, and can be used for the modelling of very hot water spectra up to the ultraviolet region.

For infrared frequencies and temperatures up to 2000 K the overall absorption modelled by POKAZATEL is very similar to the one by BT2 (Barber et al. 2006), although the accuracy of individual lines is significantly improved as illustrated by Tables 1 and 2. In particular, we note that recent, independent laboratory studies at room temperature (Campargue et al. 2017; Kassi et al. 2018) and in flames (Rutkowski et al. 2018) have strongly endorsed the accuracy of the POKAZATEL predictions. At short wavelengths and higher temperatures the completeness of the present line list results in significant opacity differences from BT2.

An important aspect of comprehensive line lists is the treatment of pressure broadening. The ExoMol project recently developed a pressure-broadening diet (Barton et al. 2017) aimed at including the effect of broadening by H_2 and He at high temperatures. Particular attention has been paid to the broadening of water spectra (Faure et al. 2013; Barton et al. 2017). We note that the implementation used within the ExoMol project allows for the treatment of pressure broadening to be transferred between line lists and hence also to the POKAZATEL line list. All data, including pressure broadening ones, can be found in the ExoMol database (Tennyson et al. 2016).

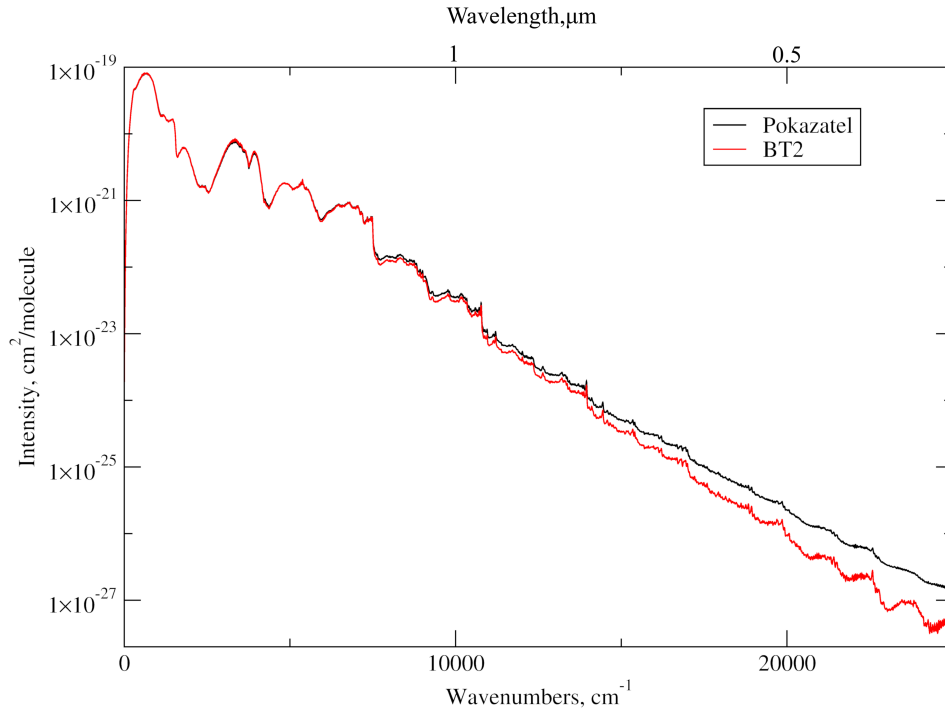


Figure 2. Comparison of absorption by H_2^{16}O predicted by BT2 and POKAZATEL at $T = 4000$ K; note the increased absorption with POKAZATEL and flattened structures.

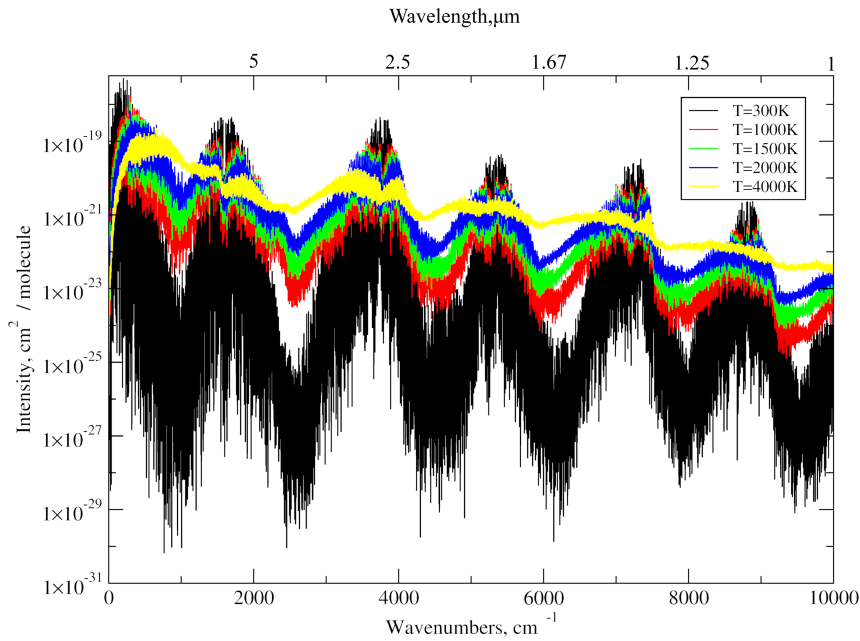


Figure 3. Temperature dependence of the absorption cross-sections of the POKAZATEL line list computed. Cross sections become increasingly flattened with increasing temperature.

7 ACKNOWLEDGEMENT

This work was supported by the ERC Advanced Investigator Project 267219, the UK Natural Environment Research Council and the Russian Fund for Fundamental Studies (grant 18-02-0057).

REFERENCES

- Abia C., Palmerini S., Busso M., Cristallo S., 2012, *Astron. Astrophys.*, 548, A55
- Alberti M., Weber R., Mancini M., Fateev A., Clausen S., 2015, *J. Quant. Spectrosc. Radiat. Transf.*, 157, 14
- Allard F., 2014, in Booth M., Matthews B. C., Graham J. R., eds, *IAU Symposium Vol. 299 of IAU Symposium, The BT-Settl Model Atmospheres for Stars, Brown Dwarfs and Planets*. pp 271–272
- Allard F., Hauschildt P. H., Miller S., Tennyson J., 1994, *Astrophys. J.*, 426, L39
- Azzam A. A. A., Yurchenko S. N., Tennyson J., Naumenko O. V., 2016, *Mon. Not. R. Astron. Soc.*, 460, 4063
- Banerjee D. P. K., Barber R. J., Ashok N. K., Tennyson J., 2005, *Astrophys. J.*, 627, L141
- Barber R. J., Miller S., Stallard T., Tennyson J., Hirst P., Carroll T., Adamson A., 2007, *Icarus*, 187, 167
- Barber R. J., Strange J. K., Hill C., Polyansky O. L., Mellau G. C., Yurchenko S. N., Tennyson J., 2014, *Mon. Not. R. Astron. Soc.*, 437, 1828
- Barber R. J., Tennyson J., Harris G. J., Tolchenov R. N., 2006, *Mon. Not. R. Astron. Soc.*, 368, 1087
- Barletta P., Shirin S. V., Zobov N. F., Polyansky O. L., Tennyson J., Valeev E. F., Császár A. G., 2006, *J. Chem. Phys.*, 125, 204307
- Barton E. J., Hill C., Czurylo M., Li H.-Y., Hyslop A., Yurchenko S. N., Tennyson J., 2017, *J. Quant. Spectrosc. Radiat. Transf.*, 203, 490
- Barton E. J., Hill C., Yurchenko S. N., Tennyson J., Dudaryonok A., Lavrentieva N. N., 2017, *J. Quant. Spectrosc. Radiat. Transf.*, 187, 453
- Beaulieu J. P., Kipping D. M., Batista V., Tinetti G., Ribas I., Noriega-Crespo S. C. J. A., Griffith C. A., Campanella G., Dong S., Tennyson J., Barber R. J., Deroo P., Fossey S. J., Liang D., Swain M. R., Yung Y., 2010, *Mon. Not. R. Astron. Soc.*, 409, 963
- Birk M., Wagner G., Loos J., Lodi L., Polyansky O. L., Kyuberis A. A., Zobov N. F., Tennyson J., 2017, *J. Quant. Spectrosc. Radiat. Transf.*, 203, 88
- Birkby J. L., de Kok R. J., Brogi M., de Mooij E. J. W., Schwarz H., Albrecht S., Snellen I. A. G., 2013, *Mon. Not. R. Astron. Soc.*, 436, L35
- Bordbar M. H., Wecl G., Hyppanen T., 2014, *Cumbust. Flame*, 161, 2435
- Boyarkin O. V., Koshelev M. A., Aseev O., Maksyutenko P., Rizzo T. R., Zobov N. F., Lodi L., Tennyson J., Polyansky O. L., 2013, *Chem. Phys. Lett.*, 568-569, 14
- Brogi M., de Kok R. J., Birkby J. L., Schwarz H., Snellen I. A. G., 2014, *Astron. Astrophys.*, 565, A124
- Bubukina I. I., Polyansky O. L., Zobov N. F., Yurchenko S. N., 2011, *Optics Spectrosc.*, 110, 160
- Campargue A., Mikhailenko S. N., Vasilchenko S., Reynaud C., Beguier S., Cermak P., Mondelain D., Kassı S., Romanini D., 2017, *J. Quant. Spectrosc. Radiat. Transf.*, 189, 407
- Carney J. R., Lightstone J. M., Piecuch S., Koch J. D., 2011, *Measure. Sci. Tech.*, 22, 045601
- Child M. S., Weston T., Tennyson J., 1999, *Mol. Phys.*, 96, 371
- Choi S. E., Light J. C., 1992, *J. Chem. Phys.*, 97, 7031
- Császár A. G., Czako G., Furtenbacher T., Tennyson J., Szalay V., Shirin S. V., Zobov N. F., Polyansky O. L., 2005, *J. Chem. Phys.*, 122, 214305
- Császár A. G., Mátyus E., Szidarovszky T., Lodi L., Zobov N. F., Shirin S. V., Polyansky O. L., Tennyson J., 2010, *J. Quant. Spectrosc. Radiat. Transf.*, 111, 1043
- Dello Russo N., Bonev B. P., DiSanti M. A., Gibb E. L., Mumma M. J., Magee-Sauer K., Barber R. J., Tennyson J., 2005, *Astrophys. J.*, 621, 537
- Dello Russo N., DiSanti M. A., Magee-Sauer K., Gibb E. L., Mumma M. J., Barber R. J., Tennyson J., 2004, *Icarus*, 168, 186
- Faure A., Wiesenfeld L., Tennyson J., Drouin B. J., 2013, *J. Quant. Spectrosc. Radiat. Transf.*, 116, 79
- Fraine J., Deming D., Benneke B., Knutson H., Jordan A., Espinoza N., Madhusudhan N., Wilkins A., Todorov K., 2014, *Nature*, 513, 526+
- Furtenbacher T., Szidarovszky T., Hruba J., Kyuberis A. A., Zobov N. F., Polyansky O. L., Tennyson J., Császár A. G., 2016, *J. Phys. Chem. Ref. Data*, 45, 043104
- Gamache R. R., Roller C., Lopes E., Gordon I. E., Rothman L. S., Polyansky O. L., Zobov N. F., Kyuberis A. A., Tennyson J., Yurchenko S. N., Császár A. G., Furtenbacher T., Huang X., Schwenke D. W., Lee T. J., Drouin B. J., Tashkun S. A., Perevalov V. I., Kochanov R. V., 2017, *J. Quant. Spectrosc. Radiat. Transf.*, 203, 70

- Gordon I. E., et al. 2017, *J. Quant. Spectrosc. Radiat. Transf.*, 203, 3
- Gray M. D., Baudry A., Richards A. M. S., Humphreys E. M. L., Sobolev A. M., Yates J. A., 2016, *Mon. Not. R. Astron. Soc.*, 456, 374
- Grechko M., Boyarkin O. V., Rizzo T. R., Maksyutenko P., Zobov N. F., Shirin S., Lodi L., Tennyson J., Császár A. G., Polyansky O. L., 2009, *J. Chem. Phys.*, 131, 221105
- Grechko M., Maksyutenko P., Zobov N. F., Shirin S. V., Polyansky O. L., Rizzo T. R., Boyarkin O. V., 2008, *J. Phys. Chem. A*, 112, 10539
- Hirota T., Kim M. K., Honma M., 2012, *Astrophys. J. Lett.*, 757, L1
- Hirota T., Kim M. K., Honma M., 2016, *Astrophys. J.*, 817, 168
- Iyer A. R., Swain M. R., Zelle M. R., Line M. R., Roudier G., Rocha G., Livingston J. H., 2016, *Astrophys. J.*, 823, 109
- Jennings D. E., Sada P. V., 1998, *Science*, 279, 844
- Kassi S., Stoltmann T., Casado M., Daeron M., Campargue A., 2018, *J. Chem. Phys.*, 148, 054201
- Kranendonk L. A., An X., Caswell A. W., Herold R. E., Sanders S. T., Huber R., Fujimoto J. G., Okura Y., Urata Y., 2007, *Optics Express*, 15, 15115
- Kyuberis A. A., Zobov N. F., Naumenko O. V., Voronin B. A., Polyansky O. L., Lodi L., Liu A., Hu S.-M., Tennyson J., 2017, *J. Quant. Spectrosc. Radiat. Transf.*, 203, 175
- Lamouroux J., Tashkun S. A., Tyuterev V. G., 2008, *Chem. Phys. Lett.*, 452, 225
- Lampel J., Pöhler D., Polyansky O. L., Kyuberis A. A., Zobov N. F., Tennyson J., Lodi L., Frieß U., Wang Y., Beirle S., Platt U., Wagner T., 2017, *Atmos. Chem. Phys.*, 17, 1271
- Li G., Guo H., 2001, *J. Mol. Spectrosc.*, 210, 90
- Lodi L., Tennyson J., 2008, *J. Quant. Spectrosc. Radiat. Transf.*, 109, 1219
- Lodi L., Tennyson J., Polyansky O. L., 2011, *J. Chem. Phys.*, 135, 034113
- Lodi L., Tolchenov R. N., Tennyson J., Lynas-Gray A. E., Shirin S. V., Zobov N. F., Polyansky O. L., Császár A. G., van Stralen J., Visscher L., 2008, *J. Chem. Phys.*, 128, 044304
- Maksyutenko P., Muentner J. S., Zobov N. F., Shirin S. V., Polyansky O. L., Rizzo T. R., Boyarkin O. V., 2007, *J. Chem. Phys.*, 126, 241101
- Melin S. T., Sanders S. T., 2016, *J. Quant. Spectrosc. Radiat. Transf.*, 180, 184
- Mizus I. I., Kyuberis A. A., Zobov N. F., Makhnev V. Y., Polyansky O. L., Tennyson J., 2018, *Phil. Trans. Royal Soc. London A*, 376, 20170149
- Mussa H. Y., Tennyson J., 1998, *J. Chem. Phys.*, 109, 10885
- Neale L., Miller S., Tennyson J., 1996, *Astrophys. J.*, 464, 516
- Partridge H., Schwenke D. W., 1997, *J. Chem. Phys.*, 106, 4618
- Pavanello M., Adamowicz L., Alijah A., Zobov N. F., Mizus I. I., Polyansky O. L., Tennyson J., Szidarovszky T., Császár A. G., Berg M., Petrigiani A., Wolf A., 2012, *Phys. Rev. Lett.*, 108, 023002
- Pavlenko Y. V., Evans A., Kerr T., Yakovina L., Woodward C. E., Lynch D., Rudy R., Pearson R. L., Russell R. W., 2008, *Astron. Astrophys.*, 485, 541
- Polyansky O. L., Jensen P., Tennyson J., 1996, *J. Chem. Phys.*, 105, 6490
- Polyansky O. L., Kyuberis A. A., Lodi L., Tennyson J., Ovsyannikov R. I., Zobov N., 2017, *Mon. Not. R. Astron. Soc.*, 466, 1363
- Polyansky O. L., Ovsyannikov R. I., Kyuberis A. A., Lodi L., Tennyson J., Zobov N. F., 2013, *J. Phys. Chem. A*, 117, 96339643
- Polyansky O. L., Zobov N. F., Tennyson J., Lotoski J. A., Bernath P. F., 1997, *J. Mol. Spectrosc.*, 184, 35
- Polyansky O. L., Zobov N. F., Viti S., Tennyson J., 1998, *J. Mol. Spectrosc.*, 189, 291
- Polyansky O. L., Zobov N. F., Viti S., Tennyson J., Bernath P. F., Wallace L., 1997, *Astrophys. J.*, 489, L205
- Rajpurohit A. S., Reyle C., Allard F., Scholz R. D., Homeier D., Schultheis M., Bayo A., 2014, *Astron. Astrophys.*, 564, A90
- Rein K. D., Sanders S. T., 2010, *Appl. Optics*, 49, 4728
- Rothman L. S., Gordon I. E., Barber R. J., Dothe H., Gamache R. R., Goldman A., Perevalov V. I., Tashkun S. A., Tennyson J., 2010, *J. Quant. Spectrosc. Radiat. Transf.*, 111, 2139
- Rutkowski L., Foltynowicz A., Johansson A. C., Khodabakhsh A., Schmidt F. M., Kyuberis A. A., Zobov N. F., Polyansky O. L., Yurchenko S. N., Tennyson J., 2018, *J. Quant. Spectrosc. Radiat. Transf.*, 205, 213
- Ryde N., Lambert J., Farzone M., Richter M. J., Josselin E., Harper G. M., Eriksson K., Greathouse T. K., 2015, *Astron. Astrophys.*, 573, A28
- Ryde N., Richter M. J., Harper G. M., Eriksson K., Lambert D. L., 2006, *Astrophys. J.*, 645, 652
- Schermaul R., Learner R. C. M., Canas A. A. D., Brault J. W., Polyansky O. L., Belmiloud D., Zobov N. F., Tennyson J., 2002, *J. Mol. Spectrosc.*, 211, 169
- Schwenke D. W., 2001, *J. Phys. Chem. A*, 105, 2352
- Shirin S. V., Polyansky O. L., Zobov N. F., Barletta P., Tennyson J., 2003, *J. Chem. Phys.*, 118, 2124

- Shirin S. V., Polyansky O. L., Zobov N. F., Ovsyannikov R. I., Császár A. G., Tennyson J., 2006, *J. Mol. Spectrosc.*, 236, 216
- Shirin S. V., Zobov N. F., Ovsyannikov R. I., Polyansky O. L., Tennyson J., 2008, *J. Chem. Phys.*, 128, 224306
- Sonnabend G., Wirtz D., Schieder R., Bernath P., 2006, *Solar Phys.*, 233, 205
- Tennyson J., Bernath P. F., Brown L. R., Campargue A., Carleer M. R., Császár A. G., Daumont L., Gamache R. R., Hodges J. T., Naumenko O. V., Polyansky O. L., Rothman L. S., Vandaele A. C., Zobov N. F., Al Derzi A. R., Fábri C., Fazliev A. Z., Furtenbacher T., Gordon I. E., Lodi L., Mizus I. I., 2013, *J. Quant. Spectrosc. Radiat. Transf.*, 117, 29
- Tennyson J., Bernath P. F., Brown L. R., Campargue A., Carleer M. R., Császár A. G., Daumont L., Gamache R. R., Hodges J. T., Naumenko O. V., Polyansky O. L., Rothman L. S., Toth R. A., Vandaele A. C., Zobov N. F., Fazliev A. Z., Furtenbacher T., Gordon I. E., Mikhailenko S. N., Voronin B. A., 2010, *J. Quant. Spectrosc. Radiat. Transf.*, 111, 2160
- Tennyson J., Bernath P. F., Brown L. R., Campargue A., Carleer M. R., Császár A. G., Gamache R. R., Hodges J. T., Jenouvrier A., Naumenko O. V., Polyansky O. L., Rothman L. S., Toth R. A., Vandaele A. C., Zobov N. F., Daumont L., Fazliev A. Z., Furtenbacher T., Gordon I. E., Mikhailenko S. N., Shirin S. V., 2009, *J. Quant. Spectrosc. Radiat. Transf.*, 110, 573
- Tennyson J., Bernath P. F., Brown L. R., Campargue A., Császár A. G., Daumont L., Gamache R. R., Hodges J. T., Naumenko O. V., Polyansky O. L., Rothman L. S., Vandaele A. C., Zobov N. F., Dénes N., Fazliev A. Z., Furtenbacher T., Gordon I. E., Hu S.-M., Szidarovszky T., Vasilenko I. A., 2014b, *J. Quant. Spectrosc. Radiat. Transf.*, 142, 93
- Tennyson J., Bernath P. F., Brown L. R., Campargue A., Császár A. G., Daumont L., Gamache R. R., Hodges J. T., Naumenko O. V., Polyansky O. L., Rothman L. S., Vandaele A. C., Zobov N. F., 2014a, *Pure Appl. Chem.*, 86, 71
- Tennyson J., Hill C., Yurchenko S. N., 2013, in *6th international conference on atomic and molecular data and their applications ICAMDATA-2012* Vol. 1545 of AIP Conference Proceedings, Data structures for ExoMol: Molecular line lists for exoplanet and other atmospheres. AIP, New York, pp 186–195
- Tennyson J., Kostin M. A., Barletta P., Harris G. J., Polyansky O. L., Ramanlal J., Zobov N. F., 2004, *Comput. Phys. Commun.*, 163, 85
- Tennyson J., Miller S., Le Sueur C. R., 1993, *Comput. Phys. Commun.*, 75, 339
- Tennyson J., Yurchenko S. N., 2012, *Mon. Not. R. Astron. Soc.*, 425, 21
- Tennyson J., Yurchenko S. N., 2017, *Intern. J. Quantum Chem.*, 117, 92
- Tennyson J., Yurchenko S. N., 2018, *Atoms*, 6, 26
- Tennyson J., Yurchenko S. N., Al-Refaie A. F., Barton E. J., Chubb K. L., Coles P. A., Diamantopoulou S., Gorman M. N., Hill C., Lam A. Z., Lodi L., McKemmish L. K., Na Y., Owens A., Polyansky O. L., Rivlin T., Sousa-Silva C., Underwood D. S., Yachmenev A., Zak E., 2016, *J. Mol. Spectrosc.*, 327, 73
- Tinetti G., Vidal-Madjar A., Liang M.-C., Beaulieu J.-P., Yung Y., Carey S., Barber R. J., Tennyson J., Ribas I., Allard N., Ballester G. E., Sing D. K., Selsis F., 2007, *Nature*, 448, 169
- Tolchenov R. N., Naumenko O., Zobov N. F., Shirin S. V., Polyansky O. L., Tennyson J., Carleer M., Coheur P.-F., Fally S., Jenouvrier A., Vandaele A. C., 2005, *J. Mol. Spectrosc.*, 233, 68
- Tsuji T., 2001, *Astron. Astrophys.*, 376, L1
- Underwood D. S., Tennyson J., Yurchenko S. N., Huang X., Schwenke D. W., Lee T. J., Clausen S., Fateev A., 2016, *Mon. Not. R. Astron. Soc.*, 459, 3890
- Varandas A. J. C., 1996, *J. Chem. Phys.*, pp 3524–3531
- Vidler M., Tennyson J., 2000, *J. Chem. Phys.*, 113, 9766
- Viti S., Tennyson J., Polyansky O. L., 1997, *Mon. Not. R. Astron. Soc.*, 287, 79
- Voronin B. A., Tennyson J., Tolchenov R. N., Lugovskoy A. A., Yurchenko S. N., 2010, *Mon. Not. R. Astron. Soc.*, 402, 492
- Yurchenko S. N., Al-Refaie A. F., Tennyson J., 2018, *Astron. Astrophys.*, 614, A131
- Yurchenko S. N., Carvajal M., Jensen P., Herregodts F., Huet T. R., 2003, *Chem. Phys.*, 290, 59
- Zobov N. F., Shirin S. V., Lodi L., Silva B. C., Tennyson J., Császár A. G., Polyansky O. L., 2011, *Chem. Phys. Lett.*, 507, 48